ADVANCES IN ATMOSPHERIC SCIENCES, VOL. 39, JULY 2022, 1167–1183

• **Original Paper** •

Evaluating the Ozone Valley over the Tibetan Plateau in CMIP6 Models※

Kequan ZHANG[1], Jiakang DUAN[1], Siyi ZHAO[1], Jiankai ZHANG[*1], James KEEBLE[2,3], and Hongwen LIU[1]

[1]*Key Laboratory for Semi-Arid Climate Change of the Ministry of Education, College of Atmospheric Sciences, Lanzhou University, Lanzhou* 730000, *China*

[2]*Department of Chemistry, University of Cambridge, Cambridge CB*2 1*EW, UK*

[3]*National Centre for Atmospheric Science, Cambridge CB*2 1*EW, UK*

(Received 25 December 2020; revised 7 March 2021; accepted 8 April 2021)

ABSTRACT

Total column ozone (TCO) over the Tibetan Plateau (TP) is lower than that over other regions at the same latitude, particularly in summer. This feature is known as the "TP ozone valley". This study evaluates long-term changes in TCO and the ozone valley over the TP from 1984 to 2100 using Coupled Model Intercomparison Project Phase 6 (CMIP6). The TP ozone valley consists of two low centers, one is located in the upper troposphere and lower stratosphere (UTLS), and the other is in the middle and upper stratosphere. Overall, the CMIP6 models simulate the low ozone center in the UTLS well and capture the spatial characteristics and seasonal cycle of the TP ozone valley, with spatial correlation coefficients between the modeled TCO and the Multi Sensor Reanalysis version 2 (MSR2) TCO observations greater than 0.8 for all CMIP6 models. Further analysis reveals that models which use fully coupled and online stratospheric chemistry schemes simulate the anticorrelation between the 150 hPa geopotential height and zonal anomaly of TCO over the TP better than models without interactive chemistry schemes. This suggests that coupled chemical-radiative-dynamical processes play a key role in the simulation of the TP ozone valley. Most CMIP6 models underestimate the low center in the middle and upper stratosphere when compared with the Microwave Limb Sounder (MLS) observations. However, the bias in the middle and upper stratospheric ozone simulations has a marginal effect on the simulation of the TP ozone valley. Most CMIP6 models predict the TP ozone valley in summer will deepen in the future.

Key words: Tibetan Plateau, stratospheric ozone, ozone valley, CMIP6

Citation: Zhang, K. Q., J. K. Duan, S. Y. Zhao, J. K. Zhang, J. Keeble, and H. W. Liu, 2022: Evaluating the ozone valley over the Tibetan Plateau in CMIP6 models. *Adv. Atmos. Sci.*, **39**(7), 1167–1183, https://doi.org/10.1007/s00376-021-0442-2.

Article Highlights:

- Most CMIP6 models can capture the seasonal cycles and spatial characteristics of the TP ozone valley.
- Chemical-radiative-dynamical processes play an important role in the simulation of the TP ozone valley.
- The multi-model mean of CMIP6 simulations predicts that the TP ozone valley in summer will deepen in the future.

1. Introduction

Stratospheric ozone not only provides local heating in the stratosphere but also modulates the global radiative balance by absorbing shortwave radiation as well as absorbing and emitting longwave radiation (Ramaswamy et al., 1996; de F. Forster and Shine, 1997; Shindell et al., 1999; Zhang et al., 2018a). In addition to its radiative effects on the climate system, stratospheric ozone can affect tropospheric weather and climate through chemical-radiative-dynamical coupling processes (Sexton, 2001; Tian and Chipperfield, 2005; Nowack, et al., 2015; Xie et al., 2016). Since the discovery of the Antarctic ozone hole in 1985, the long-term changes in stratospheric ozone and its influencing factors have been widely discussed and studied by the scientific community ((World Meteorological Organization, 2018). In 1994, Zhou and Luo (1994) identified the existence of an "ozone valley" over the Tibetan Plateau (TP) in summer using the Total Ozone Mapping Spectrometer (TOMS) satellite data. This ozone valley is characterized by total column ozone (TCO) values approximately 10% lower over the TP

※ This paper is a contribution to the special issue on Third Pole Atmospheric Physics, Chemistry, and Hydrology.

* Corresponding author: Jiankai ZHANG
Email: jkzhang@lzu.edu.cn

than that over other regions at the same latitude (Kiss et al., 2007). The TP ozone valley has noticeable seasonal variations and is generally most pronounced from May to September.

Since then, further studies have been conducted to analyze the formation mechanism of the summertime TP ozone valley. The high elevation of the TP is one of the important factors which cause the ozone valley (Ye and Xu, 2003; Bian et al., 2006, 2011, 2020). Ye and Xu (2003) calculated that column compression caused by high topography alone can result in a reduction of TCO over Lhasa by a factor of ~2.54%. Furthermore, Bian et al. (2011, 2020) discovered that air column shortage by the high topography alone accounts for half of the decreased TCO values in the TP ozone valley compared to other locations. The other important factors that are responsible for the formation of the TP ozone valley are dynamic processes, including the vertical advection of ozone and air expansion due to deep thermally forced circulations (Zhou and Luo, 1994), stratosphere–troposphere mass exchange (Cong et al., 2002; Liu et al., 2003; Zhou et al., 2004; Fan et al., 2008), changes in geopotential height and circulation associated with the Asian summer monsoon (Zhou and Zhang, 2005; Guo et al., 2012; Li et al., 2020), and large-scale uplift of isentropic surfaces and tropopause height (Tian et al., 2008; Zhang et al., 2014). In addition to the summertime ozone valley, there are occasional extreme ozone lows, with TCO values less than 220 DU over the TP during winter, which are also the result of dynamical processes (Bian, 2009; Liu et al., 2010).

The aforementioned studies mainly used satellite data and ground-based observations to identify the main characteristics of the ozone valley and its influencing factors. Additionally, some studies have used numerical models to clarify the relative contributions of dynamical and chemical processes to the formation of the TP ozone valley. Using a three-dimensional chemical transport model (OSLO CTM2), Liu et al. (2003) found that troposphere-to-stratosphere transport plays a dominant role in the summertime ozone reduction seen in the upper troposphere and lower stratosphere (UTLS), while chemical processes play a minor role. Using WRF-Chem, Yan and Bian (2015) discovered that troposphere-to-stratosphere transport is controlled by deep convection induced by the Asian summer monsoon. In addition, Tian et al. (2008) using UM-SLIMCAT chemistry-climate model, pointed out that the large-scale uplift of isentropic surfaces associated with the anticyclonic circulation of the Asian monsoon also makes a significant contribution to the ozone valley, which is larger than that of chemical processes. Although numerical models are an important tool for research on the TP ozone valley, few studies have assessed the ability of climate models to accurately simulate key characteristics of the TP ozone valley, such as its spatial distribution, seasonal cycle, and interannual variation. The Coupled Model Intercomparison Project Phase 6 (CMIP6) (Eyring et al., 2015) brings together the most advanced currently available climate models in the world. This study aims to evaluate the performance of the CMIP6 models in the simulation of stratospheric ozone and the ozone valley over the TP.

The long-term trend in stratospheric ozone over the TP is also an interesting topic. Previous studies have revealed a negative trend in the TCO over the TP from 1979 to 1997, while the TP TCO after 1997 shows a slightly positive trend (although this trend was not deemed statistically significant) (Chen et al., 2017; Li et al., 2020). In contrast, the TP ozone valley, calculated as the TCO anomaly over the TP from zonal mean TCO values, exhibits no significant summertime trend (Zhou et al., 2013; Zhang et al., 2014), suggesting that the stratospheric ozone trend over the TP is essentially consistent with the ozone trends in other regions at the same latitude. The question arises as to whether the CMIP6 models can accurately reproduce the historical TP stratospheric ozone changes. Furthermore, little is known regarding the trends in stratospheric ozone over the TP and the TP ozone valley in the future. This study focuses on following questions: (1) How accurately do the CMIP6 models simulate the seasonality and interannual variations in the TCO and stratospheric ozone over the TP when compared to observations? (2) Is the summertime ozone valley over the TP and its close relationship to dynamical processes associated with the South Asian High successfully simulated in the CMIP6 models? (3) What are the future trends in stratospheric ozone over the TP, and how is the TP ozone valley projected to change? The structure of the paper is organized as follows. Section 2 describes the CMIP6 models and simulations used in this study. Long-term changes in TCO and stratospheric ozone over the TP are evaluated in section 3. Section 4 provides a comprehensive summary. Our results should inform and motivate future studies that use CMIP6 simulations to investigate stratospheric ozone changes over the TP.

2. Data and methods

2.1. *Data*

Observed TCO is derived from the Multi Sensor Reanalysis version 2 (MSR2) dataset (van der A et al., 2010). Fourteen total ozone satellite retrieval datasets from the instruments TOMS (on the satellites Nimbus-7 and Earth Probe), SBUV (Nimbus-7, NOAA-9, NOAA-11, and NOAA-16), GOME (ERS-2), SCIAMACHY (Envisat), OMI (EOS-Aura), and GOME-2 (Metop-A) were used in MSR2. Ozone profiles are obtained from the Stratospheric Water and Ozone Satellite Homogenized (SWOOSH, version 2.5), dataset for the period 1984–2014 (Davis et al., 2016) and version 4.2x Aura Microwave Limb Sounder (MLS) Level 2 data for the period of 2005–14 (Livesey et al., 2016). The SWOOSH dataset is a merged record of stratospheric ozone and water vapor measurements taken by several limb sounding and solar occultation satellites (SAGE-II/III, UARS HALOE, UARS MLS, and Aura MLS instruments). It has 31 pressure levels from 300 to 1 hPa. The TP region is defined as 27.5°–37.5°N, 75°–105°E. A summary of the mod-

Table 1. Overview of models and data available used in this study.

Model	Resolution	Stratospheric Chemistry	Ozone	Datasets
BCC-CSM2-MR	320 × 160 longitude/latitude; 46 levels; top level 1.46 hPa	Prescribed (CMIP6 dataset)	Historical SSP2-4.5 SSP5-8.5	Wu et al. (2020) Xin et al. (2019)
BCC-ESM1	128 × 64 longitude/latitude; 26 levels; top level 2.19 hPa	Prescribed (CMIP6 dataset)	Historical	Zhang et al. (2018b)
CESM2	288 × 192 longitude/latitude; 32 levels; top level 2.25 hPa	Prescribed (other)	Historical SSP2-4.5 SSP5-8.5	Danabasoglu (2019a) Danabasoglu (2019b)
CESM2-WACCM	144 × 96 longitude/latitude; 70 levels; top level 4.5×10^{-6} hPa	Interactive chemistry	Historical SSP2-4.5 SSP5-8.5	Danabasoglu (2019c) Danabasoglu (2019d)
CNRM-CM6-1	T127; Gaussian Reduced with 24572 grid points in total distributed over 128 latitude circles (with 256 grid points per latitude circle between 30°N and 30°S reducing to 20 grid points per latitude circle at 88.9°N and 88.9°S); 91 levels; top level 78.4 km	Simplified online scheme	Historical SSP2-4.5 SSP5-8.5	Voldoire (2018) Voldoire (2019)
CNRM-ESM2-1	T127; Gaussian Reduced with 24572 grid points in total distributed over 128 latitude circles (with 256 grid points per latitude circle between 30°N and 30°S reducing to 20 grid points per latitude circle at 88.9°N and 88.9°S); 91 levels; top level 78.4 km	Interactive chemistry	Historical SSP2-4.5 SSP5-8.5	Seferian (2018) Seferian (2019)
E3SM-1-0	Cubed sphere spectral-element grid; 5400 elements with p=3; 1° average grid spacing; 90 × 90 × 6 longitude/latitude/cubeface; 72 levels; top level 0.1 hPa	Simplified online scheme	Historical	Bader et al. (2019)
FGOALS-g3	180 × 80 longitude/latitude; 26 levels; top level 2.19 hPa	Prescribed (CMIP6 dataset)	Historical SSP2-4.5 SSP5-8.5	Li (2019)
GFDL-CM4	360 × 180 longitude/latitude; 33 levels; top level 1 hPa	Prescribed (CMIP6 dataset)	Historical SSP2-4.5 SSP5-8.5	Guo et al. (2018a) Guo et al. (2018b)
GFDL-ESM4	360 × 180 longitude/latitude; 49 levels; top level 1 Pa	Interactive chemistry	Historical SSP2-4.5 SSP5-8.5	Krasting et al. (2018) John et al. (2018)
IPSL-CM6A-LR	144 × 143 longitude/latitude; 79 levels; top level 80 km	Prescribed (CMIP6 dataset)	Historical SSP2-4.5 SSP5-8.5	Boucher et al. (2018) Boucher et al. (2019)
MRI-ESM2-0	192 × 96 longitude/latitude; 80 levels; top level 0.01 hPa	Interactive chemistry	Historical SSP2-4.5 SSP5-8.5	Yukimoto et al. (2019a) Yukimoto et al. (2019b)
SAM0-UNICON	288 × 192 longitude/latitude; 30 levels; top level ~2 hPa	Prescribed (CMIP6 dataset)	Historical	Park and Shin (2019)
UKESM1-0-LL	192 × 144 longitude/latitude; 85 levels; top level 85 km	Interactive chemistry	Historical SSP2-4.5 SSP5-8.5	Tang et al. (2019) Good et al. (2019)

els and data available used in this study is provided in Table 1. In this study, the zonal anomaly of one variable is defined as the departure of this variable at a given location from its corresponding zonal mean.

2.2. *Models*

In this study, we evaluated TCO and stratospheric ozone mixing ratios over the TP derived from 14 models that participated in CMIP6: BCC-CSM2-MR, BCC-ESM1, CESM2, CESM2-WACCM, CNRM-CM6-1, CNRM-ESM2-1, E3SM-1-0, FGOALS-g3, GFDL-CM4, GFDL-ESM4, IPSL-CM6A-LR, MRI-ESM2-0, SAM0-UNICON, and UKESM1-0-LL. Five of these models (CESM2-WACCM, CNRM-ESM2-1, GFDL-ESM4, MRI-ESM2-0,

and UKESM1-0-LL) use fully coupled, interactive stratospheric chemistry, while two (CNRM-CM6-1 and E3SM-1-0) use a simple chemistry scheme. The remaining seven (BCC-CSM2-MR, BCC-ESM1, CESM2, FGOALS-g3, GFDL-CM4, IPSL-CM6A-LR, and SAM0-UNICON) do not include an interactive chemistry scheme and instead prescribe stratospheric ozone according to the CMIP6 ozone database (except in the case of CESM2, which prescribes ozone values from CESM2-WACCM simulations) (Keeble et al., 2020).

To evaluate long-term changes in stratospheric ozone over the TP, this study uses two types of simulations, the CMIP6 historical simulations and the Scenario MIP future simulations (O'Neill et al., 2017). The CMIP6 historical simulations run from 1850–2014, and the models are forced by common datasets based on observations that include historical changes in short-lived species and long-lived greenhouse gases (GHGs), global land use, solar forcing, and stratospheric aerosols from volcanic eruptions. This study only uses the historical simulation for the period of 1984–2014 for a comparison with the SWOOSH observations. The Scenario MIP future simulations run from 2015–2100 and follow the newly developed shared socioeconomic pathways (SSPs), which provide future emissions and land-use changes based on scenarios directly relevant to societal concerns regarding climate change impacts, adaptation, and mitigation. This study explores future ozone changes under the middle of the road (SSP2) and fossil-fueled development (SSP5) scenarios. Specifically, we use the ozone output derived from the SSP2-4.5 and SSP5-8.5 scenarios. It should be noted that the SSP2-4.5 and SSP5-8.5 simulations from BCC-ESM1, E3SM-1-0 and SAM0-UNICON are not available publicly at the time this paper was prepared.

3. Results

Figure 1 shows the spatial patterns of the zonal TCO anomalies from the zonal mean over the TP derived from the MSR2 observations and 14 CMIP6 models. All the models show negative TCO anomalies over the TP, suggesting that all the models broadly capture the ozone valley over the TP. The TP ozone valley has a similar shape to the TP topography, showing that the terrain has a significant effect on the total ozone (Bian, 2009; Bian et al., 2013). Note that the BCC-CSM2-MR, BCC-ESM1, and GFDL-ESM4 underestimate the magnitude of the ozone valley over the TP, whereas the other models, particularly the CESM2, CESM2-WACCM, MRI-ESM2-0, and UKESM1-0-LL, noticeably overestimate it (Fig. 2). In addition, the area of the ozone valley in GFDL-ESM4 is smaller than that in the other models, with the zero-contour line approaching the southern slope of the TP.

Figure 3a shows the seasonal cycle of TCO over the TP. Many models reproduce the seasonal cycle of TCO well, with low TCO values in September–October and high values in March–April. This feature is mainly caused by stronger extratropical ozone dynamical transport by the Brewer–Dobson circulation in winter and spring and weaker ozone transport in summer. Photochemical ozone loss until the end of autumn plays a secondary role (Fioletov and Shepherd, 2003). The peak value of ozone buildup simulated by SAM0-UNICON and UKESM1-0-LL occurs earlier than the observed value, while the minimum value in CNRM-CM6-1 and CNRM-ESM2-1 occurs one month earlier than that in the observations and multi-model mean. The seasonal cycle of the TP ozone valley in the observations and CMIP6 models is shown in Fig. 3b. The minimum value of the zonal anomaly of TP TCO in the MSR2 dataset is found in May because the warm air dome induced by the elevated heat source over the TP reaches its maximum in May (Ye and Xu, 2003; Tu et al., 2018). Some of the models (e.g., UKESM1-0-LL, FGOALS-g3, and GFDL-CM4) capture the minimum value in May well, while the minimum value in other models (e.g., CESM2, BCC-ESM1, and CNRM-ESM2-1) is found in June, which leads to two minimum values in multi-model mean, lasting from May into June.

Figures 3c and d show seasonal cycles of ozone mixing ratios and zonal ozone anomalies averaged between 70 and 150 hPa over the TP. The minimum value of ozone in the lower stratosphere occurs in summer, which is earlier than the TCO minimum in autumn (Fig. 3a). By contrast, the timing of the minimum value of the zonal ozone anomaly over the TP is the same as that of the ozone valley, suggesting that the low ozone center in the lower stratosphere mainly accounts for the TP ozone valley (Tian et al., 2008; Guo et al., 2012; Bian et al., 2013). While there is good agreement between the seasonal cycle of the multi-model mean of the TCO and the lower stratospheric ozone mixing ratios with those in the observations, the CMIP6 multi-model mean values are larger than the observed values (Figs. 3a, c). However, there are no significant differences in the zonal anomalies of TCO and the lower stratospheric ozone over the TP between the observed and the multi-model mean values (Figs. 3b, d), implying that systemic error was eliminated from the TP ozone valley by removing the zonal mean.

The time series of observed TCO over the TP and TCO from individual CMIP6 models as well as the CMIP6 multi-model mean are shown in Fig. 4a. While most CMIP6 models show distinct interannual variability, there is no interannual variability in CESM2 and SAM0-UNICON. Overall, the average of the multi-model mean TCO over the TP during 1984–2014 is larger than that derived from MSR2 dataset by about 10 DU (which is marked as black and dot line in Fig. 4). Observed TCO over the TP shows a minimum value in 1993 due to ozone loss induced by volcanic aerosols emitted during the eruption of Mt Pinatubo. After 1993 TCO shows a slightly positive trend, which is consistent with the previous literature (Zhou et al., 2013; Zhang et al., 2014). By contrast, the multi-model mean TCO shows a relat-

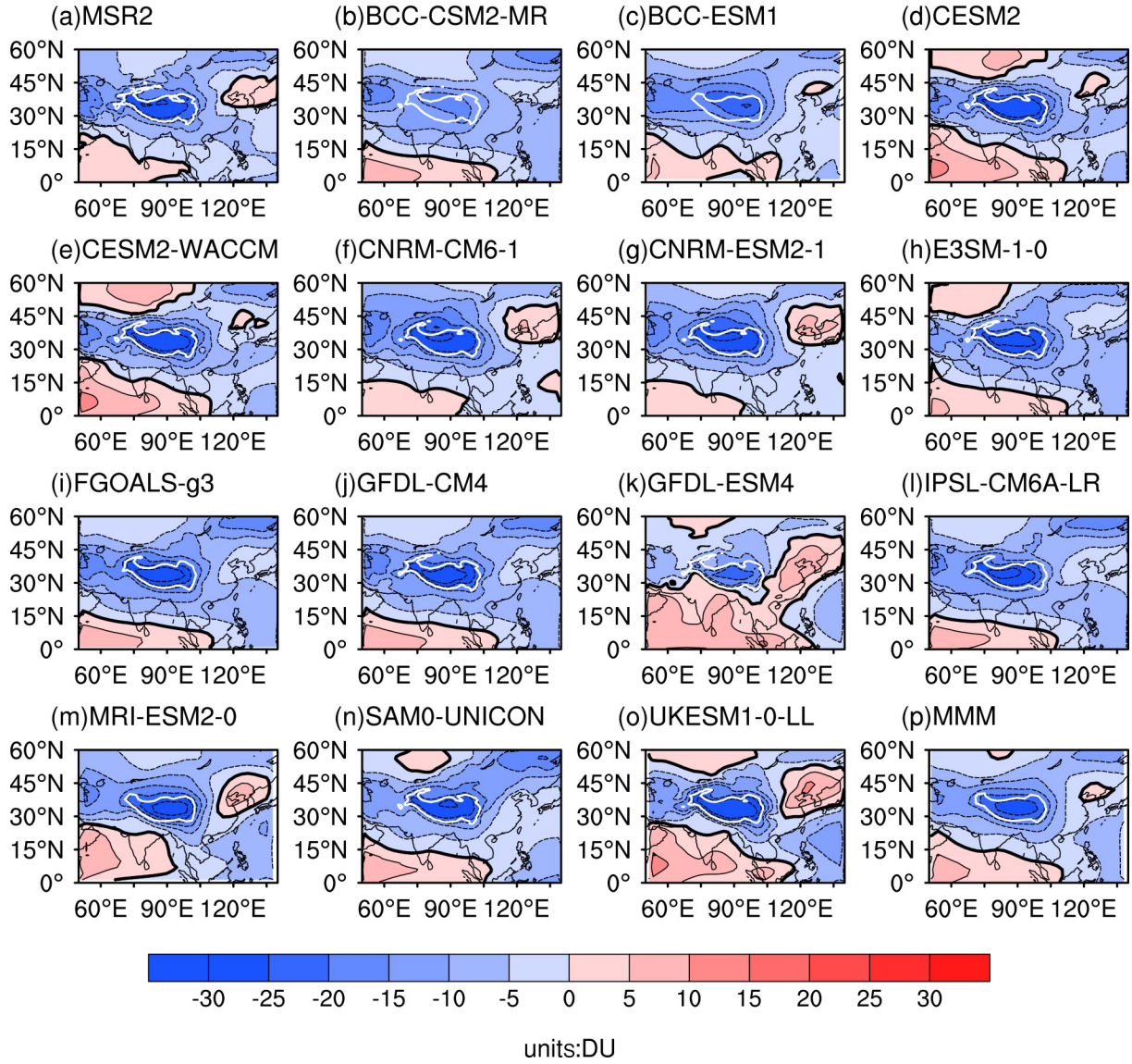

Fig. 1. June–July–August (JJA) mean total column ozone (TCO) anomalies (units: DU) from the zonal mean for the period of 1984–2014 derived from the MSR2 observations and CMIP6 models. The solid and dashed lines represent positive and negative values, respectively. The white curve line denotes the 4000 m topographical isoline.

ively weak increase, with some models (e.g., CNRM-CM6-1 and CNRM-ESM2-1) indicating a decline after the mid-1990s. Figure 4b shows the time series of the June-July-August (JJA) zonal mean TCO anomaly. The summertime ozone valley over the TP derived from the MSR2 dataset shows a negative trend without significance (Fig. 4c), consistent with the findings of Zhou et al. (2013) and Zhang et al. (2014). In contrast, nearly all CMIP6 models (except for CNRM-ESM2-1 and E3SM-1-0) show positive trends in the JJA mean ozone valley, corresponding to a weakening of the TP ozone valley. Eight models (BCC-CSM2-MR, BCC-ESM1, CESM2, CNRM-ESM2-1, GFDL-ESM4, MRI-ESM2-0, SAM0-UNICON, and UKESM1-0-LL) have positive trends that are significant at the 90% confidence level, leading to a significant positive trend in multi-model mean value (Fig. 4c). The reasons for the discrepancy in the trends of the summertime TP ozone valley between the observations and most CMIP6 models are worthy of future research.

Taylor (2001) diagram provides a statistical summary of how quantitatively similar spatial patterns are between model simulations and observational data and has been widely used to test various aspects of model performances. Figure 5 shows the Taylor diagram for the 14 CMIP6 model performances for the zonal TCO anomaly over the TP against MSR2 dataset for 1984–2014. Overall, most of the CMIP6 models can reproduce the basic spatial pattern of the ozone valley, with all spatial correlation coefficients being greater than 0.8. However, there is a large range in the ratio of the standardized interannual variances of the models to that of the observations, with BCC-CSM2-MR having the smallest ratio and MRI-ESM2-0 having the largest ratio. In

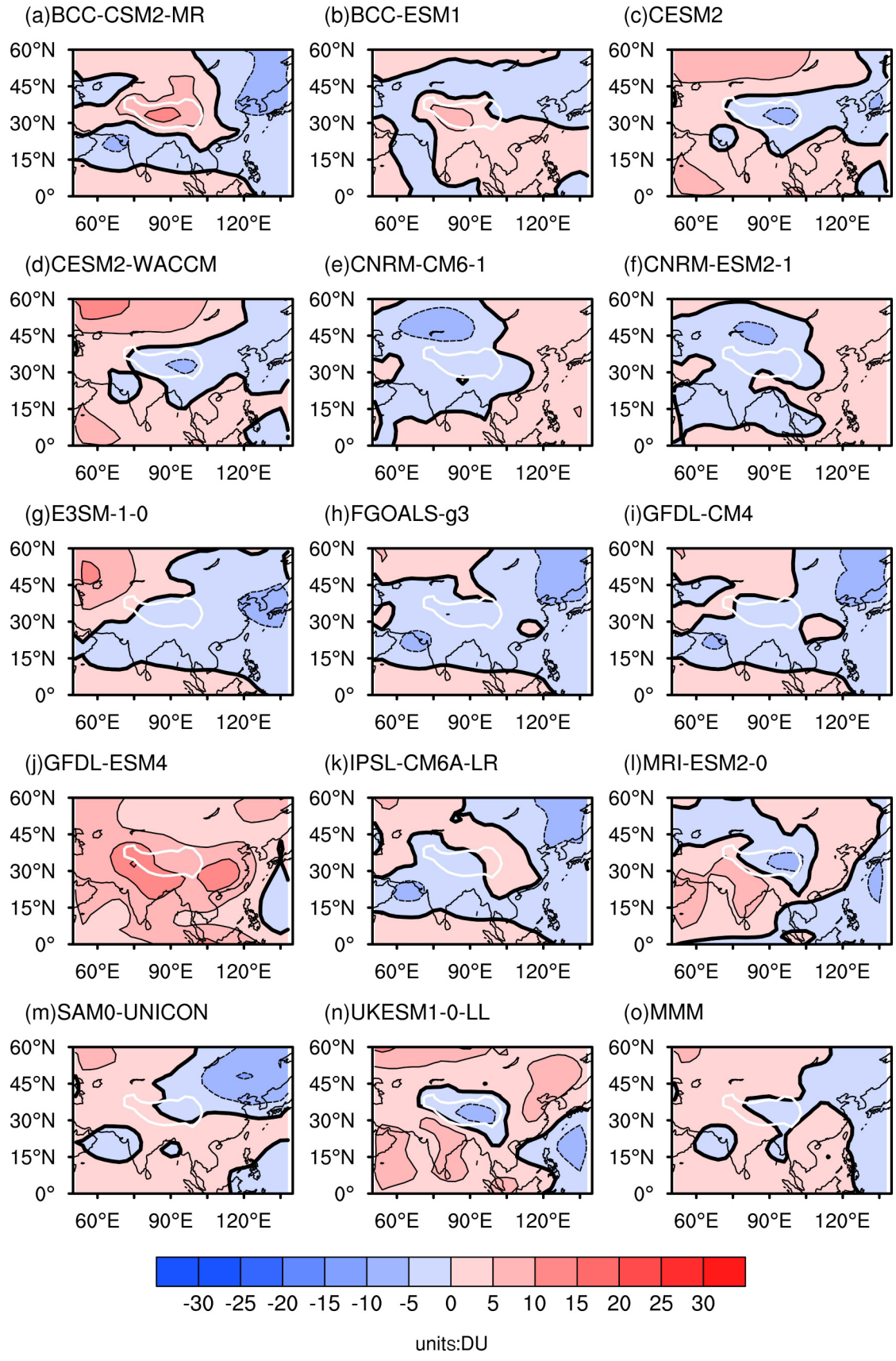

Fig. 2. JJA mean differences in zonal TCO anomalies (units: DU) between the CMIP6 models and MSR2 observations. The solid and dashed lines represent positive and negative values, respectively. The white curve line denotes the 4000 m topographical isoline.

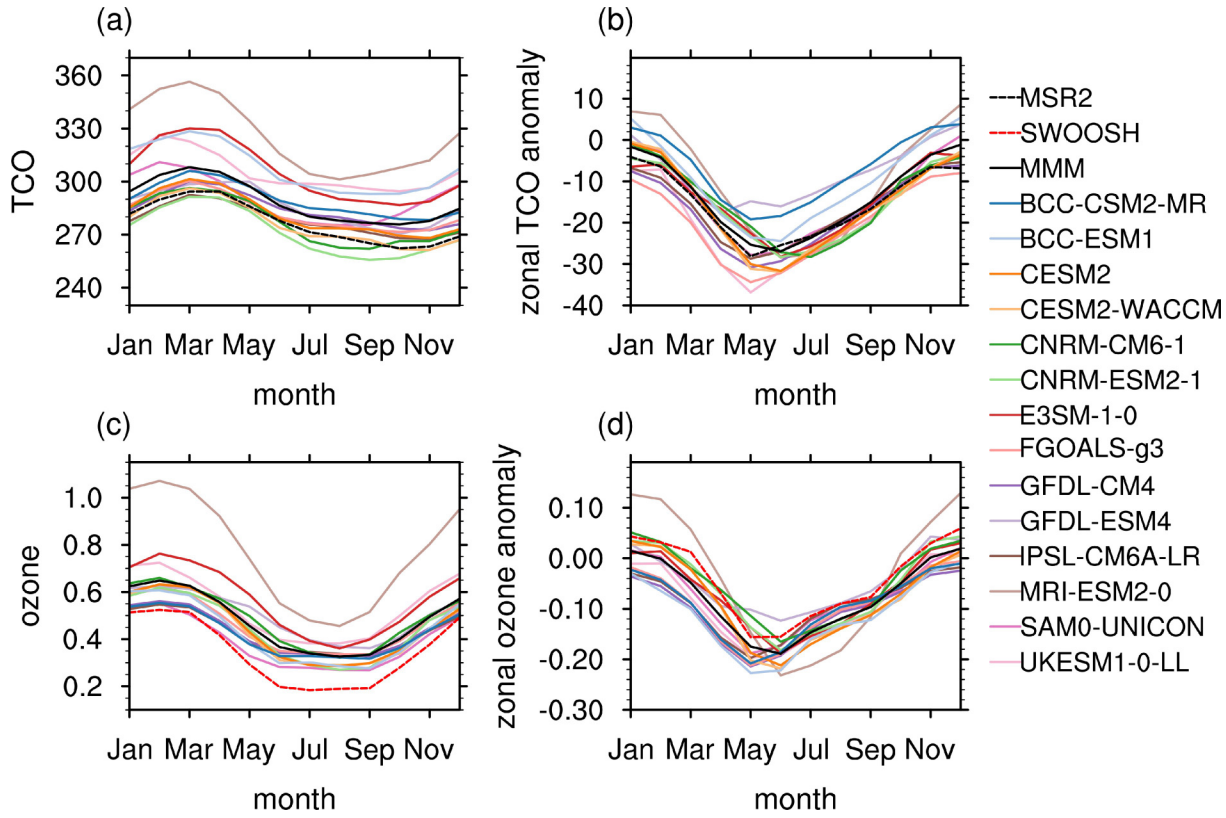

Fig. 3. The seasonal cycle of the JJA means of (a) TCO (units: DU) and (b) zonal TCO anomalies (units: DU) over the TP for the period of 1984–2014 derived from the MSR2 observation and CMIP6 models. The seasonal cycle of the JJA mean (c) ozone (units: ppmv) and (d) zonal ozone anomalies (units: ppmv) from the zonal mean in the layer between 70 and 150 hPa over the TP for the period of 1984–2014 derived from the SWOOSH observations and CMIP6 models. The MMM is the multi-model mean.

addition, compared to the MSR2 dataset, the BCC-CSM2-MR, BCC-ESM1, and GFDL-ESM4 have positive biases, (consistent with Fig. 2), whereas the other models have negative biases.

It has been documented that the intensity of the TP ozone valley is closely related to the strength of the South Asian High (Tian et al., 2008; Guo et al., 2012). Here, we use geopotential height at 150 hPa over the TP (27.5°–37.5°N, 75°–105°E, hereafter referred to as HGT150) to measure the intensity of South Asian High within the TP. Figure 6 shows the scatter plots of HGT150 and the zonal anomaly of TCO over the TP in summer. There is a significant anticorrelation between the geopotential height and zonal TCO anomaly in the observations, with a correlation coefficient of −0.67, indicating that a stronger South Asian High reduces TCO over the TP. This is because an elevated tropopause height leads to an uplift of streamlines and an upward shift of ozone vertical profiles over the TP and reduce the TP ozone column. This anticorrelation is captured by CESM2-WACCM, CNRM-CM6-1, CNRM-ESM2-1, E3SM-1-0, GFDL-ESM4, MRI-ESM2-0, and UKESM1-0-LL, while three models (CESM2, IPSL-CM6A-LR and SAM0-UNICON) simulate unrealistic positive correlations between HGT150 and the intensity of the TP ozone valley. Additionally, CESM2 and CESM2-WACCM, simulate a stronger geopotential height over the TP and stronger ozone valley than those of the observations (Figs. 6d, e, o), and vice versa for GFDL-ESM4 (Fig. 6k), which is in agreement with Fig. 2. Although CESM2-WACCM and CESM2 have similar high biases, CESM2-WACCM performs better than CESM2 in the simulation of the anticorrelation between HGT150 and the ozone valley intensity. One possible reason is that CESM2-WACCM uses fully coupled and interactive stratospheric chemistry, while CESM2 prescribes stratospheric ozone. Indeed, the five fully coupled and interactive stratospheric chemistry models (CESM2-WACCM, CNRM-ESM2-1, GFDL-ESM4, MRI-ESM2-0, and UKESM1-0-LL) simulate the anticorrelation better than the other models that lack an interactive chemistry scheme (Fig. 6p), suggesting that chemical-radiative-dynamical processes play a key role in the simulation of the TP ozone valley.

Guo et al. (2015) highlight that in addition to the ozone low in the UTLS, a low ozone anomaly exists in the upper stratosphere, i.e., there are lower ozone mixing ratios in the upper stratosphere over the TP than over other regions at the same latitude. Using a vertical integration of the MLS and CMIP6 ozone profiles between 1 and 20 hPa, Fig. 7 shows the ozone low in the upper stratosphere. The magnitude of this ozone column low (~1 DU) is smaller than

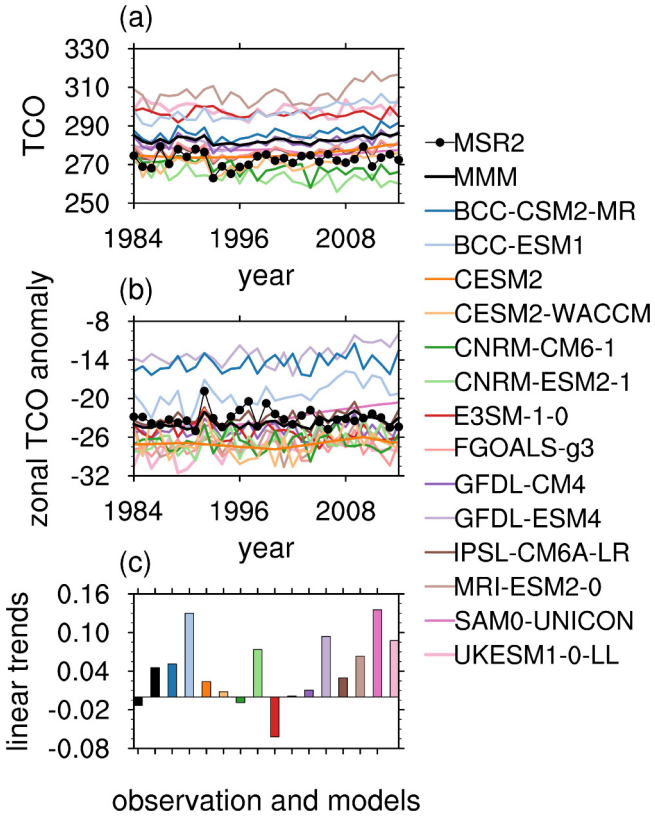

Fig. 4. Time series of JJA mean (a) TCO (units: DU) and (b) zonal TCO anomalies (units: DU) over the TP for the period of 1984–2014 derived from the MSR2 observations and CMIP6 models; and (c) Linear trends in zonal TCO anomalies over the TP for the period of 1984–2014 derived from the MSR2 observations and CMIP6 models. The MMM is the multi-model mean. The first and second column in (C) represent the linear trend in TCO derived from MSR2 observation and MMM, respectively.

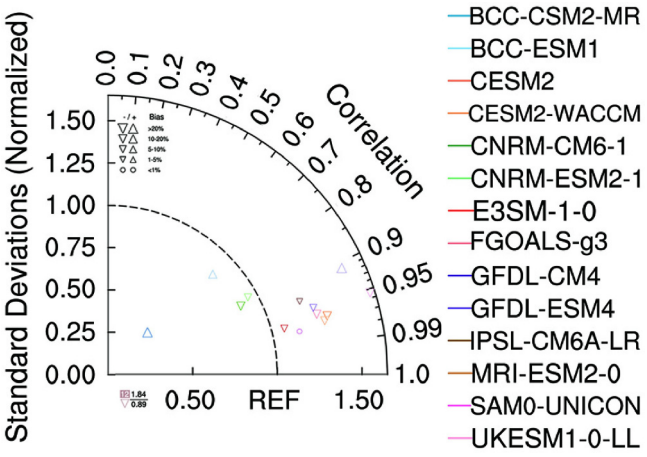

Fig. 5. Taylor diagram for JJA mean zonal TCO anomalies over the TP between the MSR2 observations and CMIP6 models for the period of 1984–2014. On the Taylor diagram, angular axes show spatial correlations between modeled and observed zonal TCO anomalies; radial axes show standard deviation (root-mean-square deviation); "REF" represents the reference line. More details please see Taylor (2001) and Keeble et al. (2020). Different symbols denote the percentage bias between observation and model. Each dot represents a model.

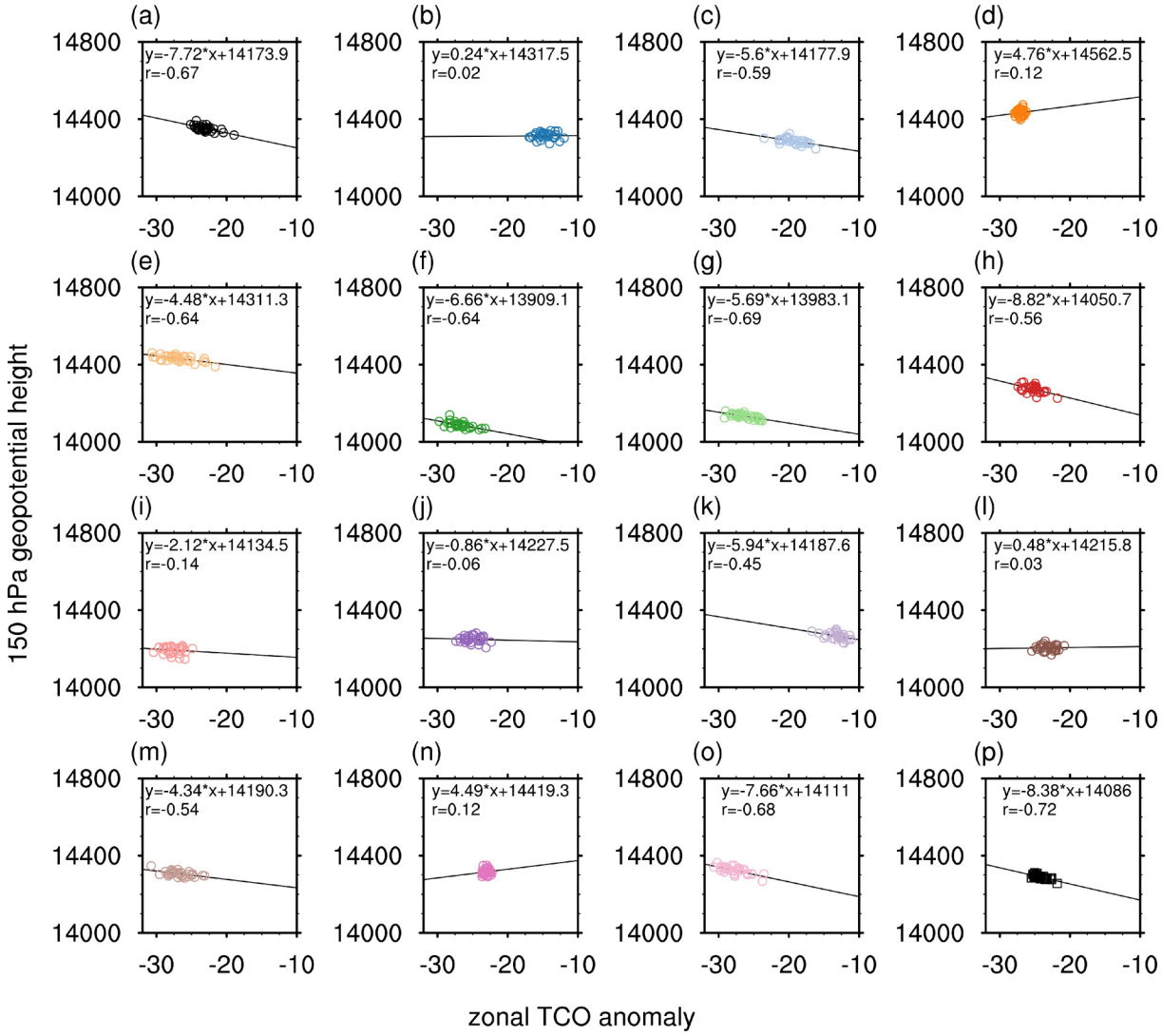

Fig. 6. Scatter plots of zonal TCO anomalies (units: DU) against 150 hPa geopotential heights (units: gpm) and their regression lines for the period of 1984–2014 derived from the MSR2 observations and CMIP6 models. Panel (p) shows the averages of zonal TCO anomalies and 150 hPa geopotential heights of five models (CESM2-WACCM, CNRM-ESM2-1, GFDL-ESM4, MRI-ESM2-0 and UKESM1-0-LL).

that of the ozone valley (more than 20 DU) over the TP in summer, which is mainly caused by dynamical processes in the UTLS. Compared with the performances of CMIP6 models in the simulations of the TP ozone valley, most models underestimate the low ozone anomaly in the upper stratosphere, leading to a weaker multi-model mean value than that in the observations. Some of the models (e.g., CNRM-ESM2-1 and E3SM-1-0) even simulate larger ozone mixing ratios in the upper stratosphere over the southern part of the TP than those over other regions at the same latitude. It is worth noting that despite the high biases of the upper stratospheric ozone mixing ratios identified in CNRM-ESM2-1 and E3SM-1-0, these models still accurately simulate the TP ozone valley (Fig. 5).

Figure 8a shows the seasonal cycle of the upper stratospheric (1–20 hPa) partial ozone column over the TP. Overall, most of the CMIP6 models capture the seasonal cycle of the TP partial ozone column well, with the maximum value in summer, which is due to the high solar zenith angle and stronger ozone photolysis production in this season. The seasonal cycle of the zonal anomaly of the partial ozone column in the upper stratosphere over the TP is shown in Fig. 8b. The difference in the zonal anomaly of the partial ozone column between the MLS and multi-model mean values is smaller than that for TCO, particularly in summer, further supporting the notion that CMIP6 models can simulate the summertime ozone valley better than they can simulate the absolute TCO value over the TP. Additionally, the zonal anomaly of the partial ozone column reaches its minimum value in summer, in contrast to the timing of the TCO minimum in May (Fig. 3b). The valley of the upper stratospheric ozone column over the TP may be caused by photochemical reactions involving chlorine species, including chlorine atoms (Cl) and chlorine monoxide (ClO), which are

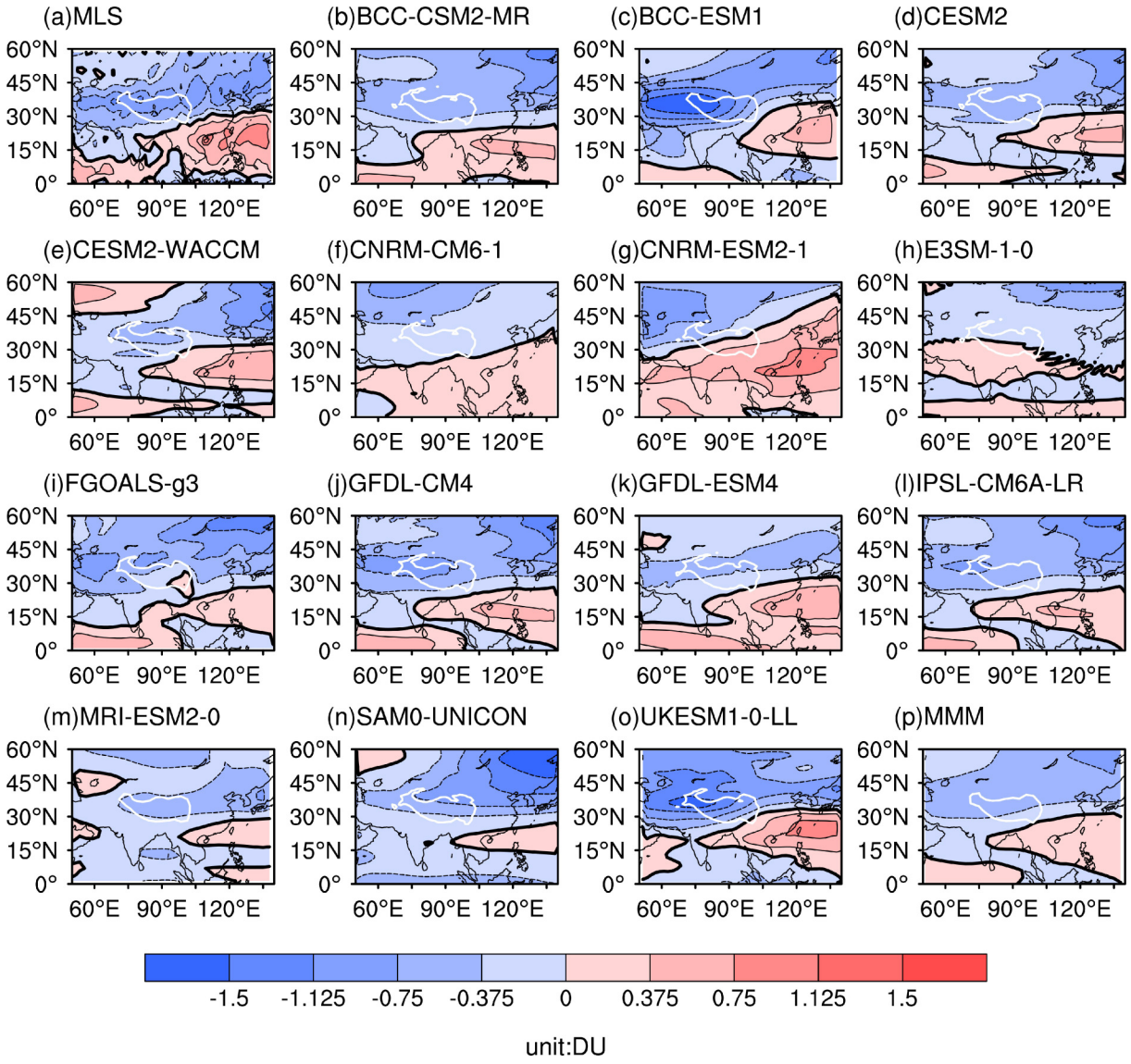

Fig. 7. June–July–August mean partial column ozone anomalies (units: DU) from the zonal mean between 1 and 20 hPa for the period of 2005–14 derived from the MLS observation and CMIP6 models. The solid and dashed lines represent positive and negative values, respectively. The white curve line denotes the 4000 m topographical isoline. The MMM is the multi-model mean.

more active in summer (Guo et al., 2015).

Figure 9a shows ozone between 1 and 20 hPa over the TP derived from observations and the CMIP6 models. Upper stratospheric ozone over the TP has similar interannual variability in the MLS and SWOOSH datasets, although ozone mixing ratios in the MLS dataset are larger than those in the SWOOSH dataset. Overall, the interannual variability of upper stratospheric ozone is smaller than that of lower stratospheric ozone because the variation in upper stratospheric ozone is dominated by chemical rather than dynamical processes (Randel and Cobb, 1994). SWOOSH ozone mixing ratios at 1–20 hPa shows a negative trend before 2002, while after 2002 no significant trend is seen, consistent with the conclusions of the WMO (World Meteorological Organization, 2018). Many CMIP6 models broadly capture this trend, although some of the models overestimate the TP upper stratospheric ozone value (e.g., GFDL-CM4 and SAM0-UNICON), while some noticeably underestimate it (e.g., GFDL-ESM4). Figure 9b shows the zonal anomaly of the upper stratospheric ozone over the TP. Most models can reproduce the negative ozone anomalies in the upper stratosphere, corresponding to the secondary low ozone center over the TP. However, CNRM-ESM2-1 and E3SM-1-0 fail to capture this feature, which is consistent with the positive anomaly over the TP in these models (Fig. 7). The interannual variability of the CMIP6 models after 2004 is similar to that of the SWOOSH and MLS data, while the variability of the SWOOSH data before 2004 is much larger than that of the models, which may be related to the limited number of ozone profiles over the TP before 2004 in the SWOOSH data (Davis et al., 2016).

Figure 10 shows the vertical distribution of the JJA

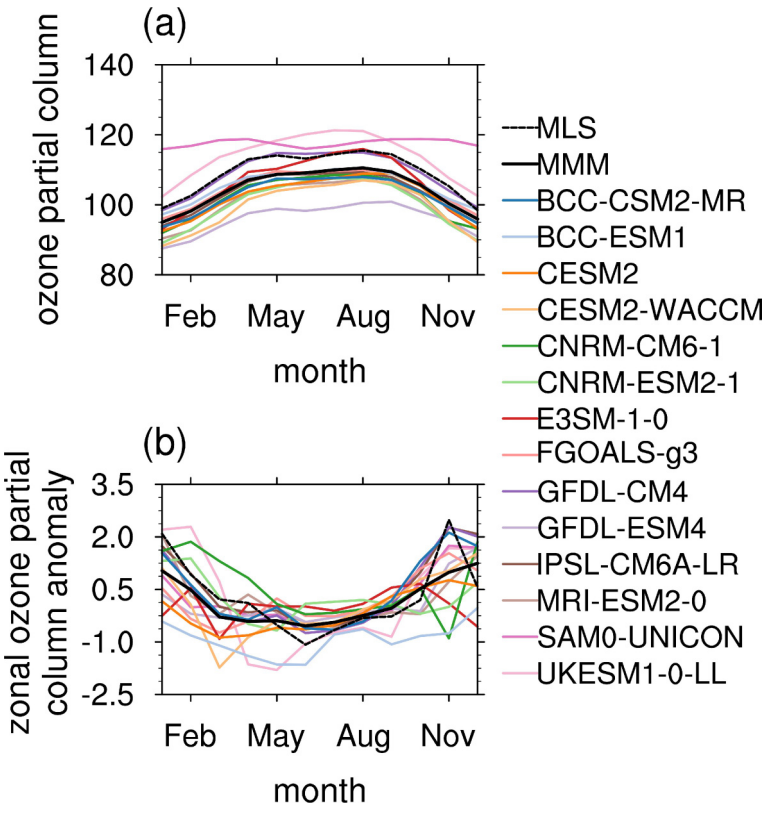

Fig. 8. The seasonal cycle of (a) partial column ozone between 1 and 20 hPa (units: DU) and (b) its zonal anomalies (units: DU) over the TP for the period of 2005–14 derived from the MLS observation and CMIP6 models. The MMM is the multi-model mean.

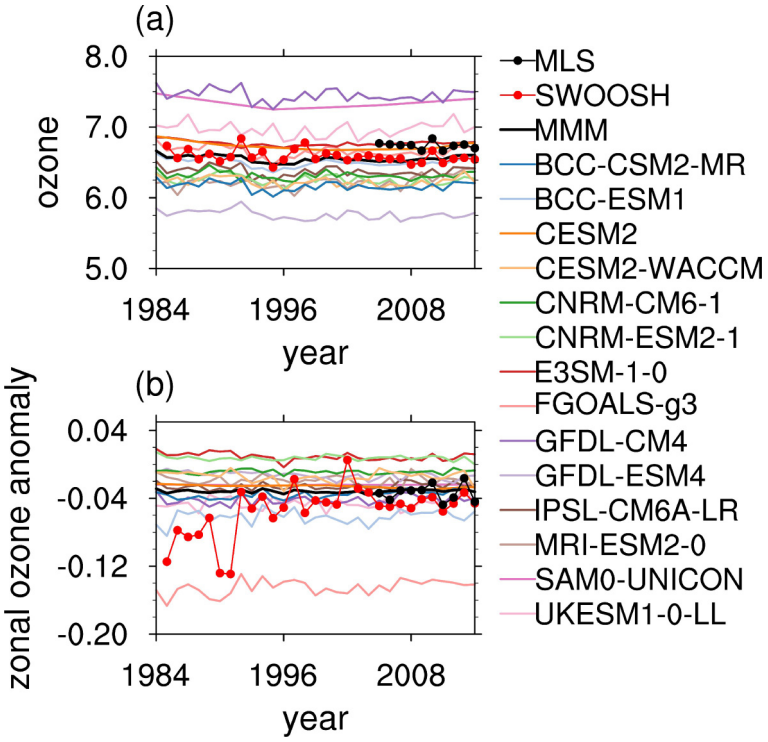

Fig. 9. Time series of JJA mean (a) ozone (units: ppmv) and (b) zonal ozone anomalies (units: ppmv) averaged between 1 and 20 hPa over the TP for the period 2005–14 derived from the MLS and SWOOSH observations and CMIP6 models. The MMM is the multi-model mean.

mean zonal anomaly of stratospheric ozone over the TP derived from the SWOOSH data and CMIP6 models. The SWOOSH results show two low centers compared with the zonal mean, one in the UTLS and the other in the middle and upper stratosphere. The multi-model mean generally captures the lower ozone concentrations in the UTLS, and the simulated magnitudes are nearly the same as those in the SWOOSH data, which are up to −0.2 ppmv at 70 hPa. However, compared to the observations, the multi-model mean underestimates the low ozone anomaly in the middle and upper stratosphere. This feature is consistent with Fig. 7, which shows that most CMIP6 models simulate weak negative or even positive ozone anomalies in the middle and upper stratosphere over the TP. Figure 10b shows the simulated vertical profile of the zonal ozone anomaly derived from the individual CMIP6 models. Most CMIP6 models reproduce the features of two low centers except for FGOALS-g3, which has noticeably negative and positive biases in the simulation of the upper and middle stratospheric ozone, respectively. The CESM2, MRI-ESM2-0, and UKESM1-0 overestimate the negative ozone anomalies in the UTLS above the TP, while the GFDL-ESM4 underestimates it, which is in agreement with the positive bias in the simulation of the TP ozone valley by the GFDL-ESM4 (Figs. 2 and 5). In addition, the low ozone center in the UTLS simulated by some of the models (E3SM-1-0 and GFDL-ESM4), shows a downward shift to 100 hPa compared to that at 70 hPa in the SWOOSH data.

Figure 11 shows the projected changes in TCO and ozone valley over the TP under the SSP2-4.5 and SSP5-8.5 scenarios. The multiple-model trend is near zero in the two future scenarios considered here, but there is a large range of trends simulated by the individual CMIP6 models. For example, the MRI-ESM2-0 simulates negative TCO trends while the CNRM-ESM2-1 simulates positive TCO trends from 2020 to 2100 under both the SSP2-4.5 and SSP5-8.5 scenarios (Figs. 11a, b). Increased greenhouse gases in the stratosphere not only cause stratospheric cooling and super ozone recovery (Brasseur and Hitchman, 1988; Rind et al., 1990; Pitari et al., 1992; Randel and Cobb, 1994; Danilin et al., 1998; Butchart and Scaife, 2001) but also accelerate tropical upwelling in the lower stratosphere (Keeble et al., 2017; He and Zhou, 2020), leading to ozone decreases in the tropics and subtropics (Huang et al., 2020). Thus, the discrepancy among different models may be related to the offsetting effects between these two processes. On the other hand, the summertime ozone valley over the TP shows significant negative trends in the future, and the decline is faster under SSP5-8.5 (−0.12 DU yr^{-1}, significant at the 99% confidence level) than under SSP2-4.5 (−0.06 DU yr^{-1}, significant at the 99% confidence level). Figure 12 shows the future changes in the geopotential height at 150 hPa over the TP derived from the SSP2-4.5 and SSP5-8.5 experiments (Figs. 12a, b). Note that the 150 hPa geopotential height over the TP will increase for the period 2020-2100 under global warming, leading to a deepening of the TP ozone valley based on the analysis of Fig. 6 in the present study. We further calculated the trends in zonal anomaly of geopotential height over the TP to compare the elevation rate of geopotential height over the TP with that of the zonal mean in the future, which is shown in Figs. 12c and d. It can be also found that the zonal anomaly of geopotential height over the TP is projected to increase over the period 2020–2100 in both SSP2-4.5 and SSP5-8.5 experiments, suggesting that the increase in geopotential height over the TP will be stronger than that at the same latitude in the future. This result further supports the notion that the TP ozone valley in summer will deepen.

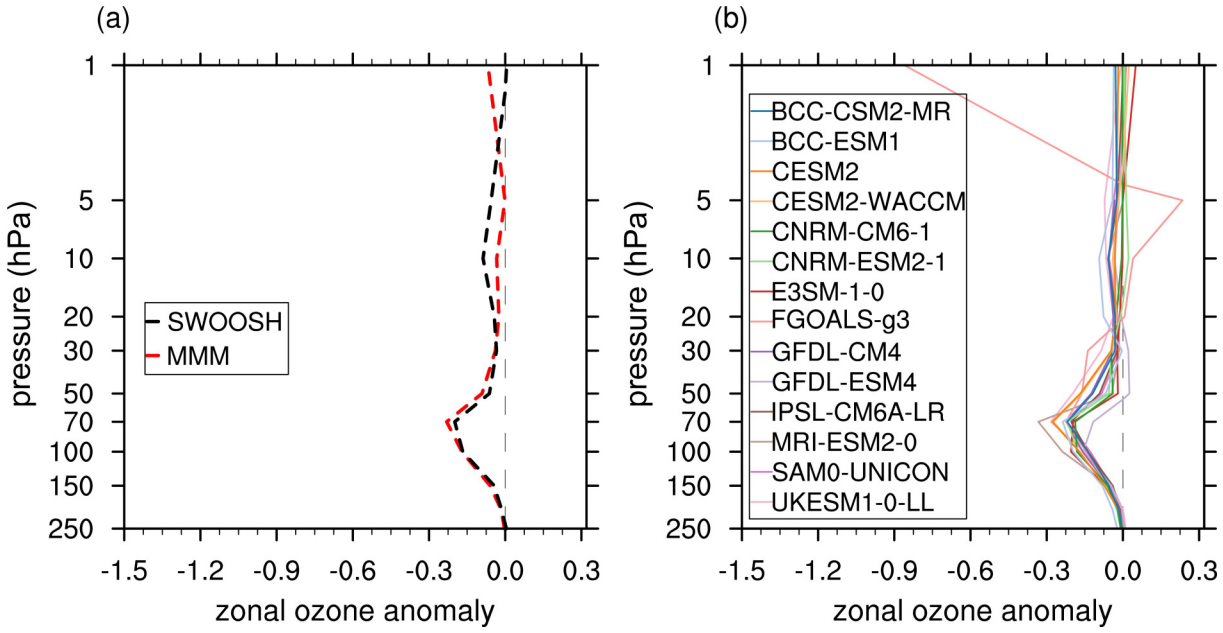

Fig. 10. Vertical profiles of JJA mean zonal ozone anomalies (units: ppmv) averaged over the TP derived from (a) the SWOOSH data (black line) and multi-model mean (MMM, red line) and (b) the CMIP6 models.

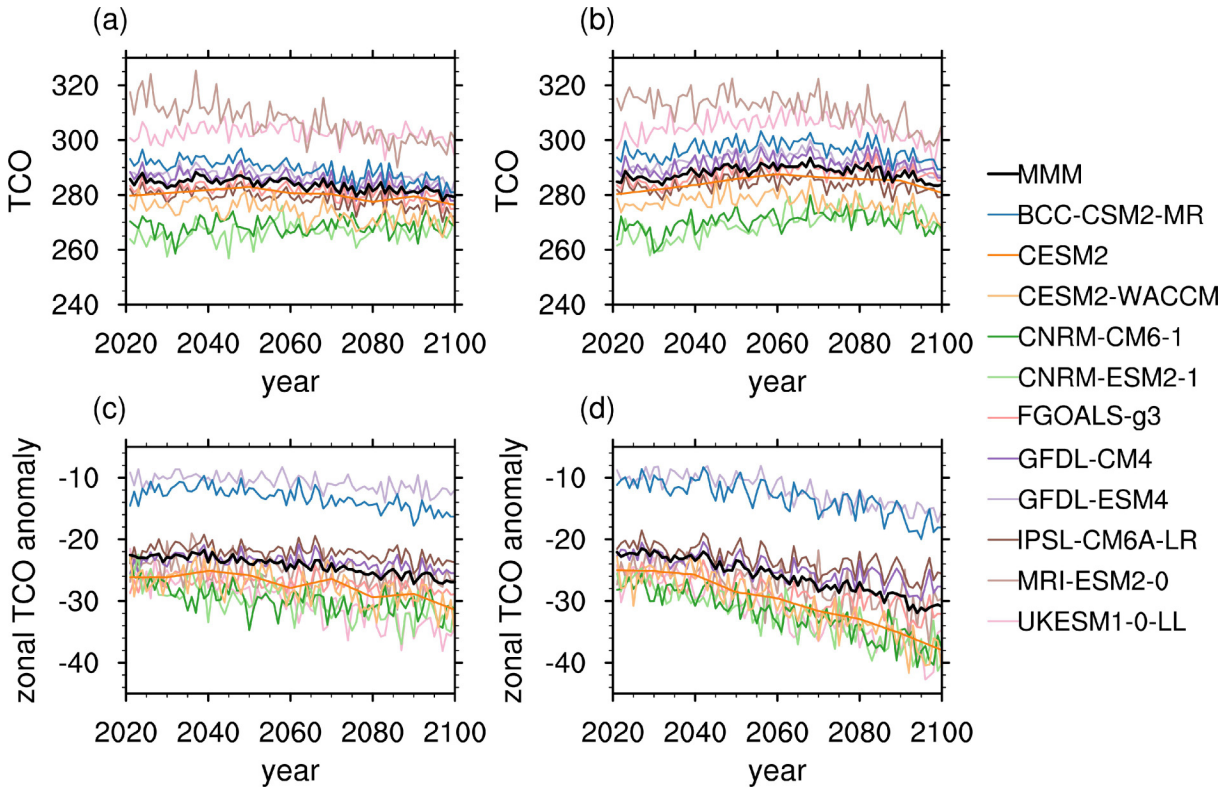

Fig. 11. Time series of JJA mean (a–b) TCO (units: DU) and (c–d) zonal TCO anomalies (units: DU) over the TP under the (a, c) SSP2-4.5 and (b, d) SSP5-8.5 scenarios.

4. Conclusions

This study evaluates the performances of available CMIP6 models in the simulation of the long-term changes in the TCO and the ozone valley over the TP and explores whether the CMIP6 models successfully simulate the dynamical relationship between the summertime ozone valley over the TP and the South Asian High. In comparison to the MSR2 dataset, the 14 CMIP6 models examined here all captured the negative TCO anomaly corresponding to the ozone valley over the TP (Fig. 1). In addition, most CMIP6 models can reproduce the spatial pattern of the ozone valley, with all spatial correlation coefficients greater than 0.8 (Fig. 5). The models also reproduce the seasonal cycles of TCO and the ozone valley over the TP well, although there are discrepancies between the CMIP6 models and observations in the timing of minimum values (Fig. 3). The summertime ozone valley derived from the MSR2 dataset shows a statistically insignificant decline for the period 1984–2014, while the CMIP6 multi-model mean shows a clear positive trend, corresponding to a weakening of the summertime ozone valley (Fig. 4). The physical mechanism responsible for this phenomenon deserves more research. In addition, most CMIP6 models have a higher bias in the interannual variance compared with that derived from the MSR2 dataset (Fig. 5).

It has previously been reported that compared with the zonal mean, there are two low ozone centers, one in the UTLS and the other in the middle and upper stratosphere. The low ozone center in the UTLS has a close relationship with the strength of the South Asian High. The CESM2-WACCM, CNRM-CM6-1, CNRM-ESM2-1, E3SM-1-0, GFDL-ESM4, MRI-ESM2-0, and UKESM1-0-LL all capture the anticorrelation between the intensities of the TP ozone valley and South Asian High, while two models (CESM2 and SAM0-UNICON) simulate unrealistic positive correlations (Fig. 6). An interesting feature is that the five fully coupled and online stratospheric chemistry models (CESM2-WACCM, CNRM-ESM2-1, GFDL-ESM4, MRI-ESM2-0, and UKESM1-0-LL) simulate the anticorrelation better than the models without an interactive chemistry scheme, suggesting that chemical-radiative-dynamical processes play a key role in the simulation of the TP ozone valley.

Most CMIP6 models underestimate the low ozone anomaly in the upper stratosphere, as noted in Guo et al. (2015) (Figs. 7 and 10). However, the low ozone anomaly in the upper stratosphere makes a minor contribution to the TP ozone valley. For example, while two models (CNRM-ESM2-1 and E3SM-1-0) simulate larger ozone concentrations in the upper stratosphere over the TP than in other regions at the same latitude, they still have higher scores in the simulation of the spatial pattern of the TP ozone valley than average, as shown in the Taylor diagram (Fig. 5).

Finally, this study explores future TCO projections for the remaining 81 years of the 21st century under the SSP2-4.5 and SSP5-8.5 scenarios (Fig. 11). TCO over the TP for

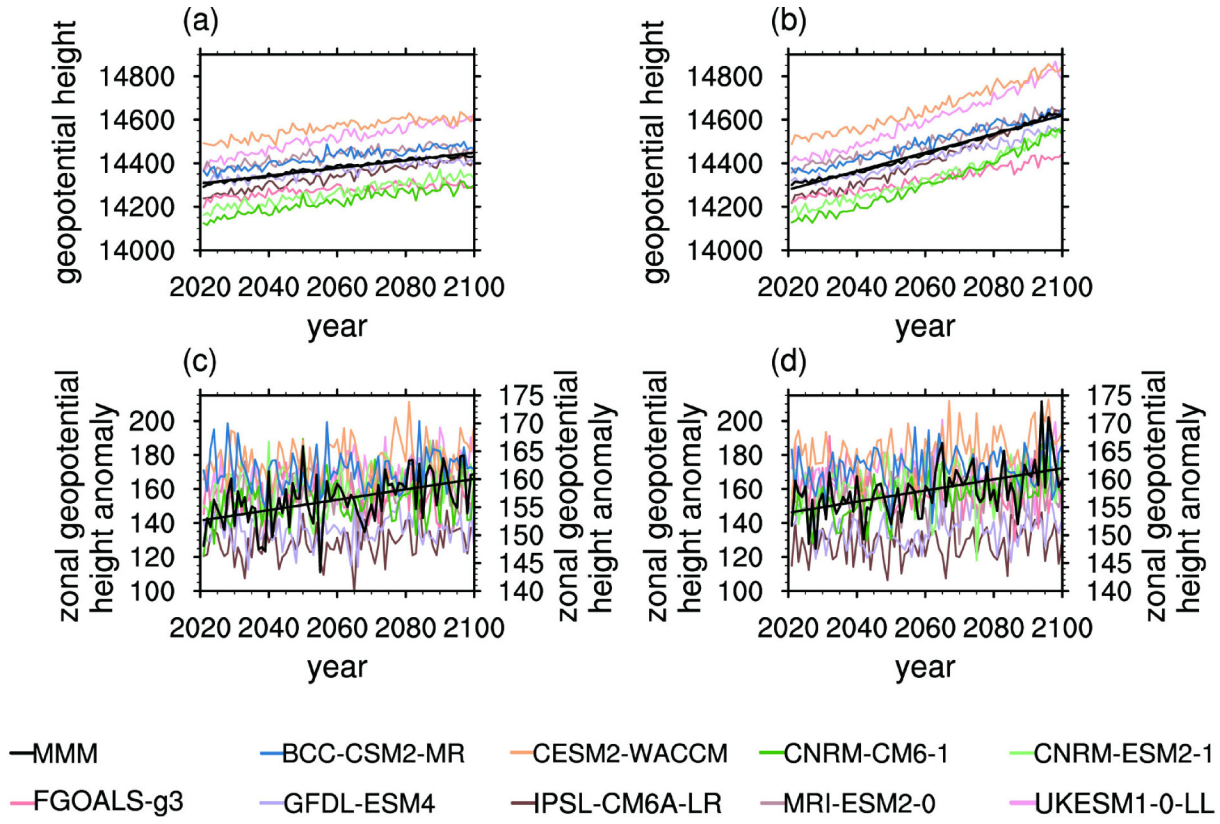

Fig. 12. Time series of JJA mean (a–b) 150 hPa geopotential height (units: gpm) and (c–d) zonal anomalies of 150-hPa geopotential height (units: gpm) over the TP under the (a-b) SSP2-4.5 and (c-d) SSP5-8.5 scenarios. The black lines in each panel represent the linear trends of MMM values. All linear trends pass the significance test at 99% confidence level. Note that the MMM value and the value of individual CMIP6 models in (c) and (d) use different vertical coordinates.

the 2020–2100 period in the case of SSP2-4.5 shows a slightly negative trend, while in the case of SSP5-8.5, it shows an insignificant positive trend. The different TCO trends between the future emission scenarios are related to the offsetting effects of ozone increases induced by stratospheric cooling and ozone reductions caused by accelerated tropical upwelling in the future. In contrast, both the SSP2-4.5 and SSP5-8.5 scenarios show a deepening of the summertime ozone valley over the TP in the future, which may be caused by the elevated geopotential height over the TP under a global warming scenario (Fig. 12).

Acknowledgements. This research was supported by the second Tibetan Plateau Scientific Expedition and Research Program (STEP, 2019QZKK0604) and the National Natural Science Foundation of China (Grant Nos. 42075062 and 91837311). This research is also supported by the Fundamental Research Funds for the Central Universities (lzujbky-2021-ey04). JK thanks NERC for financial support through NCAS. We acknowledge the World Climate Research Programme, which, through its Working Group on Coupled Modelling, coordinated and promoted CMIP6. We thank the climate modeling groups for producing and making available their model output, the Earth System Grid Federation (ESGF) for archiving the data and providing access, and the multiple funding agencies that support CMIP6 and ESGF. We thank the scientific teams for the MLS, MSR2 and SWOOSH data. The MSR2 TCO data are available from http://www.knmi.nl/kennis-en-data-centrum/publicatie/multi-sensor-reanalysis-of-total-ozone. The SWOOSH data can be downloaded from https://data.nodc.noaa.gov/cgi-bin/iso?id=gov.noaa.ncdc:C00958. The MLS data can be downloaded from https://acdisc.gesdisc.eosdis.nasa.gov/data/Aura_MLS_Level2/. The CMIP6 models can be downloaded from https://esgf-node.llnl.gov/search/cmip6/.

REFERENCES

Bader, D. C., R. Leung, M. Taylor, and R. B. McCoy, 2019: E3SM-Project E3SM1.0 model output prepared for CMIP6 CMIP historical. Version 20201101, Earth System Grid Federation, https://doi.org/10.22033/ESGF/CMIP6.4497.

Bian, J. C., 2009: Features of ozone mini-hole events over the Tibetan Plateau. *Adv. Atmos. Sci.*, **26**, 305–311, https://doi.org/10.1007/s00376-009-0305-8.

Bian, J. C., G. C. Wang, H. B. Chen, D. L. Qi, D. R. Lü, and X. J. Zhou, 2006: Ozone mini-hole occurring over the Tibetan Plateau in December 2003. *Chinese Science Bulletin*, **51**, 885–888, https://doi.org/10.1007/s11434-006-0885-y.

Bian, J. C., R. C. Yan, H. B. Chen, D. R. Lü, and S. T. Massie, 2011: Formation of the summertime ozone valley over the Tibetan Plateau: The Asian summer monsoon and air column variations. *Adv. Atmos. Sci.*, **28**, 1318–1325, https://doi.org/10.1007/s00376-011-0174-9.

Bian, J. C., Q. J. Fan, and R. C. Yan, 2013: Summertime strato-

sphere-troposphere exchange over the Tibetan plateau and its climatic impact. *Advances in Meteorological Science and Technology*, **3**, 22–28, https://doi.org/10.3969/j.issn.2095-1973.2013.02.002. (in Chinese with English abstract)

Bian, J. C., D. Li, Z. X. Bai, Q. Li, D. R. Lyu, and X. J. Zhou, 2020: Transport of Asian surface pollutants to the global stratosphere from the Tibetan Plateau region during the Asian summer monsoon. *National Science Review*, **7**, 516–533, https://doi.org/10.1093/nsr/nwaa005.

Boucher, O., and Coauthors, 2018: IPSL IPSL-CM6A-LR model output prepared for CMIP6 CMIP historical. Version 20201101, Earth System Grid Federation, https://doi.org/10.22033/ESGF/CMIP6.5195.

Boucher, O., and Coauthors, 2019: IPSL IPSL-CM6A-LR model output prepared for CMIP6 ScenarioMIP ssp126. Version 20201101, Earth System Grid Federation, https://doi.org/10.22033/ESGF/CMIP6.5262.

Brasseur, G., and M. H. Hitchman, 1988: Stratospheric response to trace gas perturbations: Changes in ozone and temperature distributions. *Science*, **240**, 634–637, https://doi.org/10.1126/science.240.4852.634.

Butchart, N., and A. A. Scaife, 2001: Removal of chlorofluorocarbons by increased mass exchange between the stratosphere and troposphere in a changing climate. *Nature*, **410**, 799–802, https://doi.org/10.1038/35071047.

Chen, S. B., L. Zhao, and Y. L. Tao, 2017: Stratospheric ozone change over the Tibetan Plateau. *Atmospheric Pollution Research*, **8**, 528–534, https://doi.org/10.1016/j.apr.2016.11.007.

Cong, C. H., W. L. Li, and X. J. Zhou, 2002: Mass exchange between stratosphere and trotosphere over the Tibetan Plateau and its surroundings. *Chinese Science Bulletin*, **47**, 508–512, https://doi.org/10.1360/02tb9117.

Danabasoglu, G., 2019a: NCAR CESM2 model output prepared for CMIP6 CMIP historical. Version 20201101, Earth System Grid Federation, https://doi.org/10.22033/ESGF/CMIP6.7627.

Danabasoglu, G., 2019b: NCAR CESM2 model output prepared for CMIP6 ScenarioMIP. Version 20201101, Earth System Grid Federation, https://doi.org/10.22033/ESGF/CMIP6.2201.

Danabasoglu, G., 2019c: NCAR CESM2-WACCM model output prepared for CMIP6 CMIP historical. Version 20201101, Earth System Grid Federation, https://doi.org/10.22033/ESGF/CMIP6.10071.

Danabasoglu, G., 2019d: NCAR CESM2-WACCM model output prepared for CMIP6 ScenarioMIP. Version 20201101, Earth System Grid Federation, https://doi.org/10.22033/ESGF/CMIP6.10026.

Danilin, M. Y., N.-D. Sze, M. K. W. Ko, J. M. Rodriguez, and A. Tabazadeh, 1998: Stratospheric cooling and Arctic ozone recovery. *Geophys. Res. Lett.*, **25**, 2141–2144, https://doi.org/10.1029/98GL01587.

Davis, S. M., and Coauthors, 2016: The Stratospheric Water and Ozone Satellite Homogenized (SWOOSH) database: A long-term database for climate studies. *Earth System Science Data*, **8**, 461–490, https://doi.org/10.5194/essd-8-461-2016.

de F. Forster, P. M., and K. P. Shine, 1997: Radiative forcing and temperature trends from stratospheric ozone changes. *J. Geophys. Res.*, **102**, 10841–10855, https://doi.org/10.1029/96JD03510.

Eyring, V., S. Bony, G. A. Meehl, C. A. Senior, B. Stevens, R. J. Stouffer, and K. E. Taylor, 2015: Overview of the Coupled Model Intercomparison Project Phase 6 (CMIP6) experimental design and organization. *Geoscientific Model Development*, **9**, 1937–1958, https://doi.org/10.5194/gmd-9-1937-2016.

Fan, W. X., W. G. Wang, and J. C. Bian, 2008: The distribution of cross-tropopause mass flux over the Tibetan Plateau and its surrounding regions. *Chinese Journal of Atmospheric Sciences*, **32**, 1309–1318, https://doi.org/10.3878/j.issn.1006-9895.2008.06.06. (in Chinese with English abstract)

Fioletov, V. E., and T. G. Shepherd, 2003: Seasonal persistence of midlatitude total ozone anomalies. *Geophys. Res. Lett.*, **30**, 1417, https://doi.org/10.1029/2002GL016739.

Good, P., A. Sellar, Y. M. Tang, S. Rumbold, R. Ellis, D. Kelley, T. Kuhlbrodt, and J. Walton, 2019: MOHC UKESM1.0-LL model output prepared for CMIP6 ScenarioMIP. Version 20201101, Earth System Grid Federation, https://doi.org/10.22033/ESGF/CMIP6.1567.

Guo, D., P. X. Wang, X. J. Zhou, Y. Liu, and W. L. Li, 2012: Dynamic effects of the South Asian high on the ozone valley over the Tibetan Plateau. *Acta Meteorologica Sinica*, **26**, 216–228, https://doi.org/10.1007/s13351-012-0207-2.

Guo, D., Y. C. Su, C. H. Shi, J. J. Xu, and A. M. Jr. Powell, 2015: Double core of ozone valley over the Tibetan Plateau and its possible mechanisms. *Journal of Atmospheric and Solar-Terrestrial Physics*, **130–131**, 127–131, https://doi.org/10.1016/j.jastp.2015.05.018.

Guo, H., and Coauthors, 2018a: NOAA-GFDL GFDL-CM4 model output historical. Version 20201101, Earth System Grid Federation, https://doi.org/10.22033/ESGF/CMIP6.8594.

Guo, H., and Coauthors, 2018b: NOAA-GFDL GFDL-CM4 model output prepared for CMIP6 ScenarioMIP. Version 20201101, Earth System Grid Federation, https://doi.org/10.22033/ESGF/CMIP6.9242.

He, C., and W. Zhou, 2020: Different enhancement of the east Asian summer monsoon under global warming and interglacial epochs simulated by CMIP6 models: Role of the subtropical high. *J. Climate*, **33**, 9721–9733, https://doi.org/10.1175/JCLI-D-20-0304.1.

Huang, X., and Coauthors, 2020: South Asian summer monsoon projections constrained by the interdecadal Pacific oscillation. *Science Advances*, **6**, eaay6546, https://doi.org/10.1126/sciadv.aay6546.

John, J. G., and Coauthors, 2018: NOAA-GFDL GFDL-ESM4 model output prepared for CMIP6 ScenarioMIP. Version 20201101, Earth System Grid Federation, https://doi.org/10.22033/ESGF/CMIP6.1414.

Keeble, J., E. M. Bednarz, A. Banerjee, N. L. Abraham, N. R. P. Harris, A. C. Maycock, and J. A. Pyle, 2017: Diagnosing the radiative and chemical contributions to future changes in tropical column ozone with the UM-UKCA chemistry–climate model. *Atmospheric Chemistry and Physics*, **17**, 13801–13818, https://doi.org/10.5194/acp-17-13801-2017.

Keeble, J., and Coauthors, 2020: Evaluating stratospheric ozone and water vapor changes in CMIP6 models from 1850-2100. *Atmospheric Chemistry and Physics-Discussions*, 1–68, https://doi.org/10.5194/acp-2019-1202.

Kiss, P., R. Müller, and I. M. Jánosi, 2007: Long-range correlations of extrapolar total ozone are determined by the global atmospheric circulation. *Nonlinear Processes in Geophysics*,

14, 435–442, https://doi.org/10.5194/npg-14-435-2007.

Krasting, J. P., and Coauthors, 2018: NOAA-GFDL GFDL-ESM4 model output prepared for CMIP6 CMIP historical. Version 20201101, Earth System Grid Federation, https://doi.org/10.22033/ESGF/CMIP6.8597.

Li, L. J., 2019: CAS FGOALS-g3 model output prepared for CMIP6 CMIP historical. Version 20201101, Earth System Grid Federation, https://doi.org/10.22033/ESGF/CMIP6.3356.

Li, Y. J., M. P. Chipperfield, W. H. Feng, S. S. Dhomse, R. J. Pope, F. Q. Li, and D. Guo, 2020: Analysis and attribution of total column ozone changes over the Tibetan Plateau during 1979–2017. *Atmospheric Chemistry and Physics*, **20**, 8627–8639, https://doi.org/10.5194/acp-20-8627-2020.

Liu, C. X., Y. Liu, Z. N. Cai, S. T. Gao, J. C. Bian, X. Liu, and K. Chance, 2010: Dynamic formation of extreme ozone minimum events over the Tibetan Plateau during northern winters 1987–2001. *J. Geophys. Res.*, **115**, D18311, https://doi.org/10.1029/2009JD013130.

Liu, Y., W. L. Li, X. J. Zhou, and J. H. He, 2003: Mechanism of formation of the ozone valley over the Tibetan Plateau in summer—Transport and chemical process of ozone. *Adv. Atmos. Sci.*, **20**, 103–109, https://doi.org/10.1007/BF03342054.

Livesey, N. J., and Coauthors, 2016: EOS MLS Version 4.2x Level 2 data quality and description document. Rev., B, Jet Propulsion Laboratory, D - 33509.

Nowack, P. J., N. L. Abraham, A. C. Maycock, P. Braesicke, J. M. Gregory, M. M. Joshi, A. Osprey, and J. A. Pyle, 2015: A large ozone-circulation feedback and its implications for global warming assessments. *Nature Climate Change*, **5**, 41–45, https://doi.org/10.1038/nclimate2451.

O'Neill, B. C., and Coauthors, 2017: The roads ahead: Narratives for shared socioeconomic pathways describing world futures in the 21st century. *Global Environmental Change*, **42**, 169–180, https://doi.org/10.1016/j.gloenvcha.2015.01.004.

Park, S., and J. Shin, 2019: SNU SAM0-UNICON model output prepared for CMIP6 CMIP historical. Version 20201101, Earth System Grid Federation, https://doi.org/10.22033/ESGF/CMIP6.7789.

Pitari, G., S. Palermi, G. Visconti, and R. G. Prinn, 1992: Ozone response to a CO_2 doubling: Results from a stratospheric circulation model with heterogeneous chemistry. *J. Geophys. Res.*, **97**, 5953–5962, https://doi.org/10.1029/92JD00164.

Ramaswamy, V., M. D. Schwarzkopf, and W. J. Randel, 1996: Fingerprint of ozone depletion in the spatial and temporal pattern of recent lower-stratospheric cooling. *Nature*, **382**, 616–618, https://doi.org/10.1038/382616a0.

Randel, W. J., and J. B. Cobb, 1994: Coherent variations of monthly mean total ozone and lower stratospheric temperature. *J. Geophys. Res.*, **99**, 5433–5447, https://doi.org/10.1029/93JD03454.

Rind, D., R. Suozzo, N. K. Balachandran, and M. J. Prather, 1990: Climate change and the middle atmosphere. Part I: The doubled CO_2 Climate. *J. Atmos. Sci.*, **47**, 475–494, https://doi.org/10.1175/1520-0469(1990)047<0475:CCATMA>2.0.CO;2.

Seferian, R., 2018: CNRM-CERFACS CNRM-ESM2-1 model output prepared for CMIP6 CMIP historical. Version 20201101, Earth System Grid Federation, https://doi.org/10.22033/ESGF/CMIP6.4068.

Seferian, R., 2019: CNRM-CERFACS CNRM-ESM2-1 model output prepared for CMIP6 ScenarioMIP. Version 20201101, Earth System Grid Federation, https://doi.org/10.22033/ESGF/CMIP6.1395.

Sexton, D. M. H., 2001: The effect of stratospheric ozone depletion on the phase of the Antarctic Oscillation. *Geophys. Res. Lett.*, **28**, 3697–3700, https://doi.org/10.1029/2001GL013376.

Shindell, D., D. Rind, N. Balachandran, J. Lean, and P. Lonergan, 1999: Solar cycle variability, ozone, and climate. *Science*, **284**, 305–308, https://doi.org/10.1126/science.284.5412.305.

Tang, Y. M., S. Rumbold, R. Ellis, D. Kelley, J. Mulcahy, A. Sellar, J. Walton, and C. Jones, 2019: MOHC UKESM1.0-LL model output prepared for CMIP6 CMIP historical. Version 20201101, Earth System Grid Federation, https://doi.org/10.22033/ESGF/CMIP6.6113.

Taylor, K. E., 2001: Summarizing multiple aspects of model performance in a single diagram. *J. Geophys. Res.*, **106**, 7183–7192, https://doi.org/10.1029/2000JD900719.

Tian, W. S., and M. P. Chipperfield, 2005: A new coupled chemistry–climate model for the stratosphere: The importance of coupling for future O_3-climate predictions. *Quart. J. Roy. Meteor. Soc.*, **131**, 281–303, https://doi.org/10.1256/qj.04.05.

Tian, W. S., M. P. Chipperfield, and Q. Huang, 2008: Effects of the Tibetan Plateau on total column ozone distribution. *Tellus B: Chemical and Physical Meteorology*, **60**, 622–635, https://doi.org/10.1111/j.1600-0889.2008.00338.x.

Tu, H. W., H. Y. Tian, C. H. Wei, W. L. Wang, R. H. Zhang, and J. L. Luo, 2018: Impact of the east–west phase of South Asia High on water vapor distribution near tropopause over the Asian monsoon region. *Climatic and Environmental Research*, **23**, 341–354, https://doi.org/10.3878/j.issn.1006-9585.2017.17048. (in Chinese with English abstract)

van der A, R. J., M. A. F. Allaart, and H. J. Eskes, 2010: Multi sensor reanalysis of total ozone. *Atmospheric Chemistry and Physics*, **10**, 11277–11294, https://doi.org/10.5194/acp-10-11277-2010.

Voldoire, A., 2018: CMIP6 simulations of the CNRM-CERFACS based on CNRM-CM6-1 model for CMIP experiment historical. Version 20201101, Earth System Grid Federation, https://doi.org/10.22033/ESGF/CMIP6.4066.

Voldoire, A., 2019: CNRM-CERFACS CNRM-CM6-1 model output prepared for CMIP6 ScenarioMIP. Version 20201101, Earth System Grid Federation, https://doi.org/10.22033/ESGF/CMIP6.1384.

World Meteorological Organization (WMO), 2018: Executive summary: Scientific assessment of ozone depletion. Rep. No. 58, 2018 World Meteorological Organization, Global Ozone Research and Monitoring Project, Geneva, Switzerland, 67 pp.

Wu, T. W., and Coauthors, 2020: BCC BCC-CSM2MR model output prepared for CMIP6 CMIP historical. Version 20201101, Earth System Grid Federation, https://doi.org/10.22033/ESGF/CMIP6.2948.

Xie, F., and Coauthors, 2016: A connection from Arctic stratospheric ozone to El Niño-Southern oscillation. *Environmental Research Letters*, **11**, 124026, https://doi.org/10.1088/1748-9326/11/12/124026.

Xin, X. G., and Coauthors, 2019: BCC BCC-CSM2MR model output prepared for CMIP6 ScenarioMIP. Version 20201101, Earth System Grid Federation, https://doi.org/10.22033/ESGF/CMIP6.1732.

Yan, R. C., and J. C. Bian, 2015: Tracing the boundary layer sources of carbon monoxide in the Asian summer monsoon anticyclone using WRF-Chem. *Adv. Atmos. Sci.*, **32**, 943–951, https://doi.org/10.1007/s00376-014-4130-3.

Ye, Z. J., and Y. F. Xu, 2003: Climate characteristics of ozone over Tibetan Plateau. *J. Geophys. Res.*, **108**, 4654, https://doi.org/10.1029/2002JD003139.

Yukimoto, S., and Coauthors, 2019a: MRI MRI-ESM2.0 model output prepared for CMIP6 CMIP historical. Version 20201101, Earth System Grid Federation, https://doi.org/10.22033/ESGF/CMIP6.6842.

Yukimoto, S., and Coauthors, 2019b: MRI MRI-ESM2.0 model output prepared for CMIP6 ScenarioMIP. Version 20201101, Earth System Grid Federation, https://doi.org/10.22033/ESGF/CMIP6.638.

Zhang, J., and Coauthors, 2018a: BCC BCC-ESM1 model output prepared for CMIP6 CMIP historical. Version 20201101, Earth System Grid Federation, https://doi.org/10.22033/ESGF/CMIP6.2949.

Zhang, J. K., W. S. Tian, F. Xie, H. Y. Tian, J. L. Luo, J. Zhang, W. Liu, and S. Dhomse, 2014: Climate warming and decreasing total column ozone over the Tibetan Plateau during winter and spring. *Tellus B: Chemical and Physical Meteorology*, **66**, 23415, https://doi.org/10.3402/tellusb.v66.23415.

Zhang, J. K., and Coauthors, 2018b: Stratospheric ozone loss over the Eurasian continent induced by the polar vortex shift. *Nature Communications*, **9**, 206, https://doi.org/10.1038/s41467-017-02565-2.

Zhou, L. B., H. Zou, S. P. Ma, and P. Li, 2013: The Tibetan ozone low and its long-term variation during 1979–2010. *Acta Meteorologica Sinica*, **27**, 75–86, https://doi.org/10.1007/s13351-013-0108-9.

Zhou, S. W., and R. H. Zhang, 2005: Decadal variations of temperature and geopotential height over the Tibetan Plateau and their relations with Tibet ozone depletion. *Geophys. Res. Lett.*, **32**, L18705, https://doi.org/10.1029/2005GL023496.

Zhou, X. J., and C. Luo, 1994: Ozone valley over Tibetan Plateau. *Journal of Meteorological Research*, **8**, 505–506.

Zhou, X. J., W. L. Li, L. X. Chen, and Y. Liu, 2004: Study of ozone change over Tibetan Plateau. *Acta Meteorologica Sinica*, **62**, 513–527, https://doi.org/10.3321/j.issn:0577-6619.2004.05.001. (in Chinese with English abstract)